3. W. H. Lowdermilk and D. Milam, in *Excimer Lasers, Their Applications, and New Frontiers in Lasers* (SPIE, Bellingham, WA, 1984), Vol. 476, p. 143.

4. M. Kozlowski, R. Smith, and R. Wolfe, LLNL Internal Memo LDG 91-120, 19 November 1991.

5. G. E. P. Box, W. G. Hunter, and J. S. Hunter, *Statistics for Experimenters: An Introduction to Design, Data Analysis, and Model Building* (Wiley, New York, 1978).

6. W. H. Lowdermilk and D. Milam, IEEE J. Quantum Electron. **17**, 1888 (1981).

7. Dupont Co., Instruments/Biomedical Division, Newtown, CT 06470 – Model "Sorval GKM."

8. J. D. Boyer, S. R. Foltyn, B. R. Mauro, and V. E. Sanders, in *Laser Induced Damage in Optical Materials: 1989*, Natl. Inst. Stand. Technol. (U.S.), Spec. Publ. 801 (U.S. Government Printing Office, Washington, DC, 1990), p. 417.

9. B. E. Newnam, S. R. Foltyn, D. M. Gill, and L. J. Jolin, in *Laser Induced Damage in Optical Materials: 1984*, Natl. Bur. Stand. (U.S.), Spec. Publ. 727 (U.S. Government Printing Office, Washington, DC, 1986), p. 342.

10. B. Liao, D. J. Smith, and B. McIntyre, in *Laser Induced Damage in Optical Materials: 1985*, Natl. Bur. Stand. (U.S.), Spec. Publ. 746 (U.S. Government Printing Office, Washington, DC, 1988), p. 305.

2.C An Externally Triggered, Single-Mode, Nd:YLF Laser Oscillator

Single-axial mode, high-brightness laser oscillators are of considerable interest for a variety of applications from nonlinear optics to laser-fusion lasers. The latter typically require such lasers for the generation of shaped pulses with the added requirement of accurate synchronization to other short-pulse lasers.

Mono-mode lasers[1,2,3] have been reported widely in the literature over the past several years but reports on reliable mono-mode oscillators at 1053 nm (Nd:YLF) are less frequent. Recently, several reports on mono-mode lasers have taken advantage of efficient diode pumping and the recent discovery of low-loss, acousto-optically induced, unidirectional ring oscillators.[1] Unidirectional ring oscillators avoid spatial hole burning and are essential for crystalline media such as Nd:YLF, which cannot use such effective methods as are used in the unidirectional, non-planar Nd:YAG ring resonators,[3] or linear resonators using circular polarization in the active medium.[4] The diode-pumped Nd:YLF lasers reported have output energies that typically range in the μJ regime[2] with ≤ 1-kHz repetition rates, but they have not been checked for external synchronizability, i.e., build-up time jitter of the *Q*-switched output pulse.

In this article we concentrate on reliable mono-mode oscillator performance with ~1 mJ output energy at very moderate repetition rates <10 Hz. The oscillator has an externally triggered Q-switch permitting synchronization to a signal with tens-of-microseconds jitter relative to the flash-lamp trigger pulse. To this end we use a conventional, flash-lamp-pumped active medium (Nd:YLF) lasing at 1053 nm, which is ideally suited for amplification in large Nd:phosphate glass-amplifier chains. Mono-mode operation is assured using a combination of extended, low-intensity, pre-lase phase,[5–7] unidirectional ring-laser configuration, and a single, 10-mm-thick, intra-cavity etalon. The pre-lase phase is controlled with an active feedback to suppress normal mode spiking prior to Q-switching. In addition, we have installed an active, interferometric, cavity-length control.[8] This assures wavelength stability and increases the reproducibility of the laser-output characteristics such as amplitude, build-up time, and FWHM of the Q-switched pulse. Successful synchronization in this context implies a build-up time jitter of much less than the FWHM, i.e., typically <10%.

Experimental Setup

The stable, unidirectional ring cavity has an optical path length of ~86 cm (Fig. 51.26). The active medium is a 4-mm-diam, 60-mm-long, Nd:YLF rod with wedged end faces. The rod is oriented so it lases at 1053-nm wavelength. A low-pressure xenon lamp (1.5-in. arc length) is used in a diffuse, close-coupled pump cavity. Transverse modes are suppressed by a 1.5-mm aperture, and unidirectional operation is achieved with a Faraday isolator causing a ~20° rotation of the plane of polarization. A single KD*P Pockels cell ($V_{\lambda/2}$ = 8 kV) is used for controlling intracavity losses during the pre-lase period and for Q-switching. A 10-mm-thick intracavity etalon (reflectivity R = 50% at 1053 nm) suppresses higher longitudinal modes. The temperature of the etalon is controlled to approximately ±0.1°C.

All components are mounted on a completely enclosed invar table. Mechanical stability of the laser resonator is further enhanced by using heavy mounts and minimizing the number of positioning adjustments. One of the cavity mirrors is mounted on a piezoelectric translator (PZT) embedded in an Al block for stability and for suppression of low-frequency mechanical resonances.

To provide long-term stability through compensation for temperature drifts, we use an active control system incorporating a frequency-stabilized HeNe interferometer (Fig. 51.26). The 633-nm wavelength provides a resolution of almost twice that of the Nd:YLF wavelength of 1053 nm. Part of the HeNe beam is reflected at the output coupler and interferes with the remainder after one round-trip. The three high-reflectance mirrors are dichroic with R = 100% at 1053 nm and 80% at 633 nm, and the output coupler has R = 90% at 1053 nm and 25% at 633 nm. A half-wave plate and a collimator are used to optimize the HeNe fringe contrast, which also depends on the applied Pockels cell voltage. An enlarged image of the HeNe fringes is incident on two closely spaced photodiodes such that the diodes straddle a fringe. The photodiode signals are differentially amplified, processed, and fed back to the PZT (Burleigh model PZ-70 HV driver and PZT model PZ-80 with 7-μm maximum excursion). The open feedback circuit response has a dead time of $t_d \approx 200$ μs and a rise time of $t_r \approx 2$ ms. The

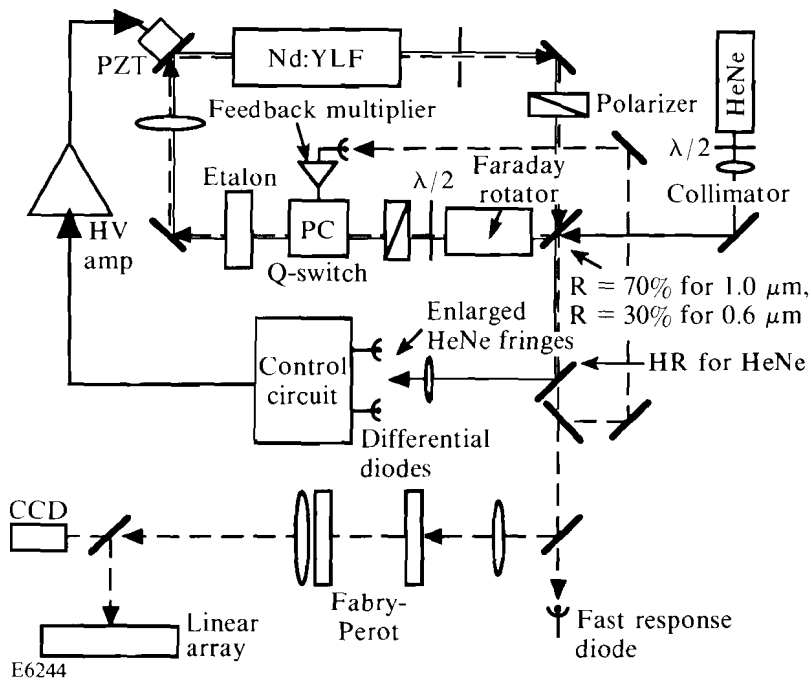

Fig. 51.26
Experimental setup for unidirectional, single-axial-mode, Nd:YLF laser with length feedback control and extended low-intensity pre-lase feedback control.

optimum operating parameters for this feedback circuit are determined using a method proposed by Oppelt.[9] The circuit has a bandwidth of ~200 Hz, enough to respond to typical long-term temperature and PZT drifts of the optical path length. The length control is not completely dispersion-free and can give rise to some residual, uncompensated error signal. This is a result of the differential wavelength-dependent, thermo-optic response of the laser and KD*P crystals, which tend to compensate each other, although not completely.

With the control loop closed, the laser can be tuned to operate at the desired wavelength by translating the entire differential diode assembly across the HeNe fringe pattern. This simple feedback system is capable of maintaining the Nd:YLF cavity length to within $\lesssim 0.2\ \lambda_{HeNe}$ over periods of several hours. The time limits on the stabilization are set by the maximum excursion of the PZT. The ambient temperature control in our experimental area was so poor as to set the ultimate limits on the time period (2 to 3 hours) before the feedback ran out of PZT travel.

Part of the 1-μm laser beam is used in another feedback loop to generate an extended pre-lase phase of $\lesssim 100$ μs. This feedback circuit is a high-voltage cascade, open-loop amplifier connected to a Pockels cell. The open-loop amplifier combined with a cascade of several decoupled MOSFET transistors allows both feedback for the pre-lase phase and for the subsequent Q-switch. The small-signal bandwidth of this system is 340 kHz (large-signal bandwidth ~130 kHz) with a typical response time of ~300 ns.

A flat-plate Fabry-Perot (FP) interferometer and a fast vacuum photodiode are used to analyze and characterize the temporal and spectral behavior of the Nd:YLF laser output.

The FP interferometer (Burleigh model RC-110) has an instrumental finesse of $F_I \approx 90$. The plate spacing of ~10 cm is chosen such that adjacent intracavity etalon modes of the Nd:YLF oscillator are centered between adjacent FP orders, while adjacent oscillator modes appear closely spaced to, but well-resolved from, adjacent FP orders. Thus, the fringe location clearly identifies its source. To avoid speckle a negative lens of short focal length (f = −5 cm) is used to illuminate the interferometer resulting in parabolic intensity distribution of the output. A 1-m lens then images the FP fringe pattern onto a linear photodiode array.

The linear photodiode array (EG&G PARC 1453 AC) has 1024 pixels with a 25-μm diode spacing and 2.5-mm diode height. The array is operated at −5°C and can achieve a dynamic range of ~15,000. The array is centered on the FP fringe pattern but its height distorts the fringes and adds asymmetric shoulders near the origin of the circular FP pattern.

The temporal behavior of the laser output is analyzed for high-frequency modulation and build-up time jitter. A vacuum photodiode (Hamamatsu R1328U-01) with a rise time of $t_r \approx 100$ ps is displayed on a 4.5-GHz Tektronix SCD 5000 transient digitizer. The cutoff frequency of the detection system is around 10 GHz, which is close to the free spectral range (FSR) of the 1-cm intracavity etalon and greatly exceeds the 350-MHz longitudinal-mode spacing of the ring resonator. The build-up time jitter of the Q-switched pulse with respect to the Q-switch trigger is monitored with a HP-4220 PIN diode and a Tektronix 2440 oscilloscope. The two scope traces and the linear-array FP data are acquired by a personal computer for subsequent statistical analysis.

Experimental Results

For diagnostic test purposes, the setup shown in Fig. 51.26 is used with the laser-output feedback loop disabled and the Q-switch optically triggered on top of the first relaxation oscillation. Varying the flash-lamp pump energy and the bias voltage on the Pockels cell, the FWHM of the Q-switched pulse can be varied between 20 and 100 ns.

Figure 51.27 shows Fabry-Perot fringes obtained with the linear array for a typical mono-mode shot and two different multi-mode shots. The center of the FP fringe pattern is to the right of the traces displayed. The top line represents a clean mono-mode shot. The shoulder to the right of each FP fringe is mostly instrumental although it may also contain a small frequency drift as a result of heating of the laser rod during the pre-lase period. This period is well below the response time of the HeNe interferometric-length control system. The dotted line is a FP trace in the presence of a weak adjacent oscillator mode, and the bottom curve shows the simultaneous presence of a neighboring oscillator mode and a neighboring mode of the intracavity etalon.

The corresponding oscilloscope traces just before the peak of the Q-switched pulse are shown in Fig. 51.28. For illustration purposes, the traces are shifted vertically. The mono-mode pulse (top line) exhibits no modulation while the middle trace shows the 340-MHz modulation typical for the presence of two neighboring oscillator modes. The bottom trace corresponds to the bottom trace in Fig. 51.27 and shows the 340-MHz modulation with a superposed weak, but clearly identifiable, 10.3-GHz modulation caused by the simultaneous presence of a second intracavity etalon mode. The amplitude of the 10.3-GHz modulation is drastically reduced by the finite bandwidth of the detection system.

For the long-term stability experiments we have chosen to analyze the FP traces only since the correspondence of the oscilloscope and FP traces has been so clearly demonstrated in Figs. 51.27 and 51.28. For these experiments the cavity-length stabilization feedback circuit is engaged. The Q-switch trigger is delayed by ~40 μs relative to the initial rise in intracavity laser intensity. However, to simulate the external trigger capability, the Q-switch is actually triggered from the flash-lamp current pulse.

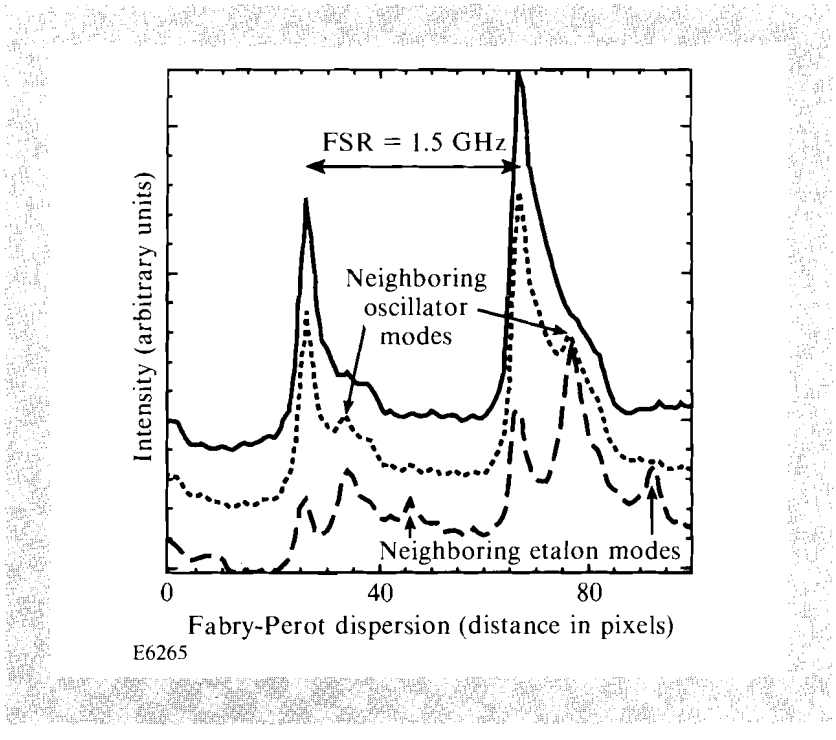

Fig. 51.27
Fabry-Perot traces taken with a linear diode array for single-mode and multi-mode emission from the oscillator. (Free spectral range of the Fabry-Perot interferometer is $\lambda_{FSR} \approx 1.5$ GHz.) The single-mode response has an extended foot on one side, which appears to be caused by heating of the laser rod during the extended pre-lase period prior to Q-switching. Multi-mode behavior of this oscillator is obtained only if the intensity-feedback control is disabled.

Figure 51.29 displays the results of a 6-h stability test where the laser was continuously operated at a 5-Hz repetition rate and data were recorded every 2 min. The figure shows a cross section of the first four FP fringes to one side of the zeroth-order fringe. The FSR of the FP is ~1.5 GHz. A small amount of slow frequency drift is clearly seen in these records but no multi-mode shots have ever been observed under these conditions. This residual frequency drift is caused by dispersion inside the laser cavity between the 1-μm laser pulse and the 633-nm HeNe interferometer. However, any mode-jumping to neighboring cavity or etalon modes is very distinct as will be seen later.

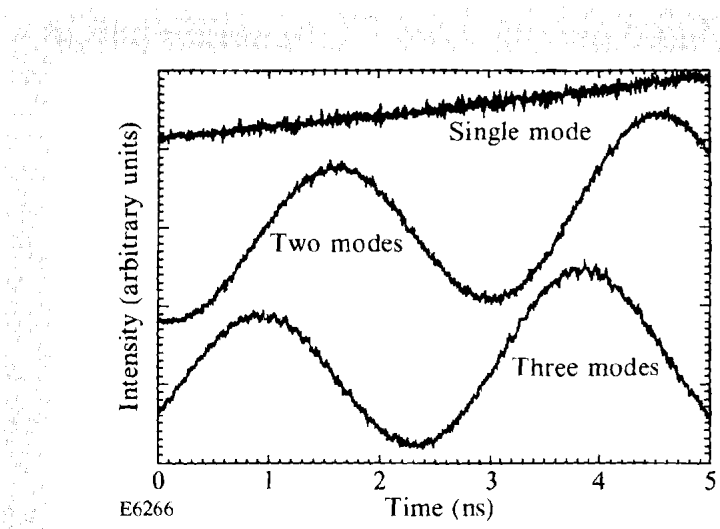

Fig. 51.28
Fast oscilloscope traces of the Q-switched laser output corresponding to the Fabry-Perot traces shown in Fig. 51.27.

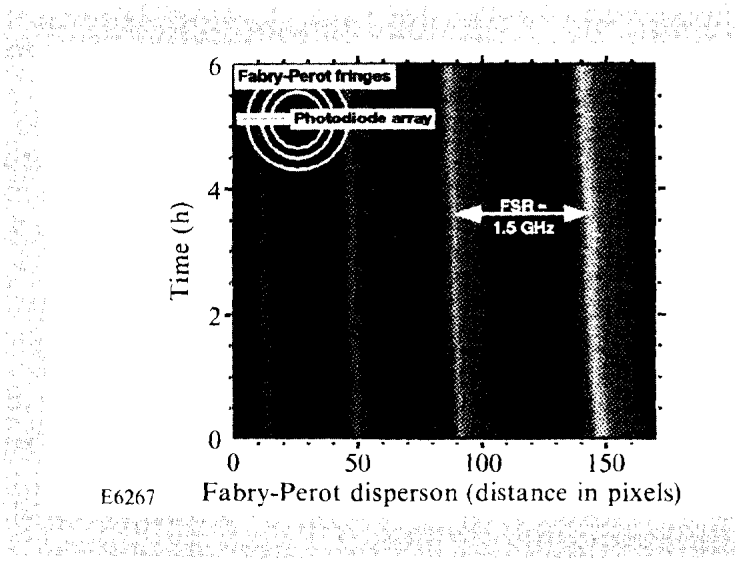

Fig. 51.29
Long-term stability test of mono-mode output: first four orders of the Fabry-Perot interferometer ($\lambda_{FSR} \approx 1.5$ GHz) taken with a linear diode array. The laser was operated at 5 Hz and data were recorded every 2 min. (For explanation of shoulders see Fig. 51.27.)

The build-up time jitter (time between Q-switch initiation and pulse peak) is shown in Fig. 51.30(a). The corresponding amplitudes and FWHM are shown in Fig. 51.30(b). For these experiments the laser is again Q-switched after a 40-μs pre-lase phase at a data acquisition rate of one shot per minute (one out of every 300 actual shots) for a total of ~160 recorded shots. The cavity-length feedback loop is active. The corresponding FP traces in Fig. 51.30(c) indicate single-mode operation with a slight frequency drift. This frequency drift reflects a change in the effective cavity length as a result of temperature rise, which could not be completely compensated by the cavity-length feedback circuit because of dispersion between 633 nm (HeNe interferometer) and 1053 nm (Nd:YLF laser). The average build-up time for this typical run is 521.45±8.40 (2%) ns, the peak intensity is 4.18±0.24 (6%) (arbitrary units), and the FWHM is 99.9±2.88 (3%) ns. The corresponding peak-to-valley (p-t-v) ranges are 39 ns, 1.12 arbitrary units (27%), and 16 ns (16%).

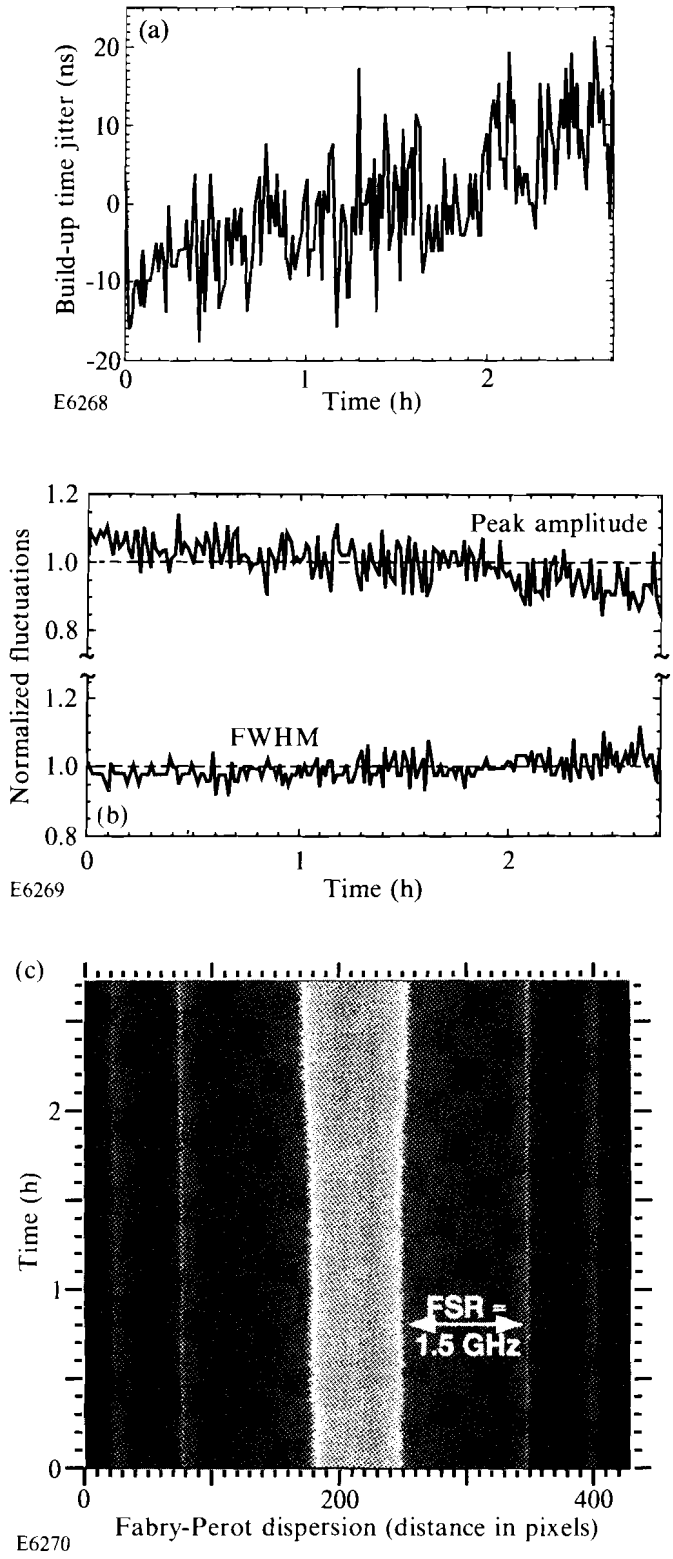

Fig. 51.30
(a) Build-up time fluctuations around the average for Q-switched pulses with active laser-cavity-length feedback control and low-intensity feedback control during the pre-lase phase for suppression of normal-mode spiking. (b) Fluctuations of the peak intensity and FWHM of the Q-switched pulses and Fabry-Perot fringe cross sections (c) for the same series of shots ($\lambda_{FSR} \approx 1.5$ GHz).

Figure 51.31 demonstrates the clear correlation between mode-hopping and fluctuations in amplitude, FWHM, and build-up time. For this purpose the cavity-length feedback circuit is disabled but the pre-lase intensity feedback control remained active. Figure 51.31 displays the results for 95 shots taken at a data acquisition rate of 1 shot per min (one out of every 300 actual shots). The

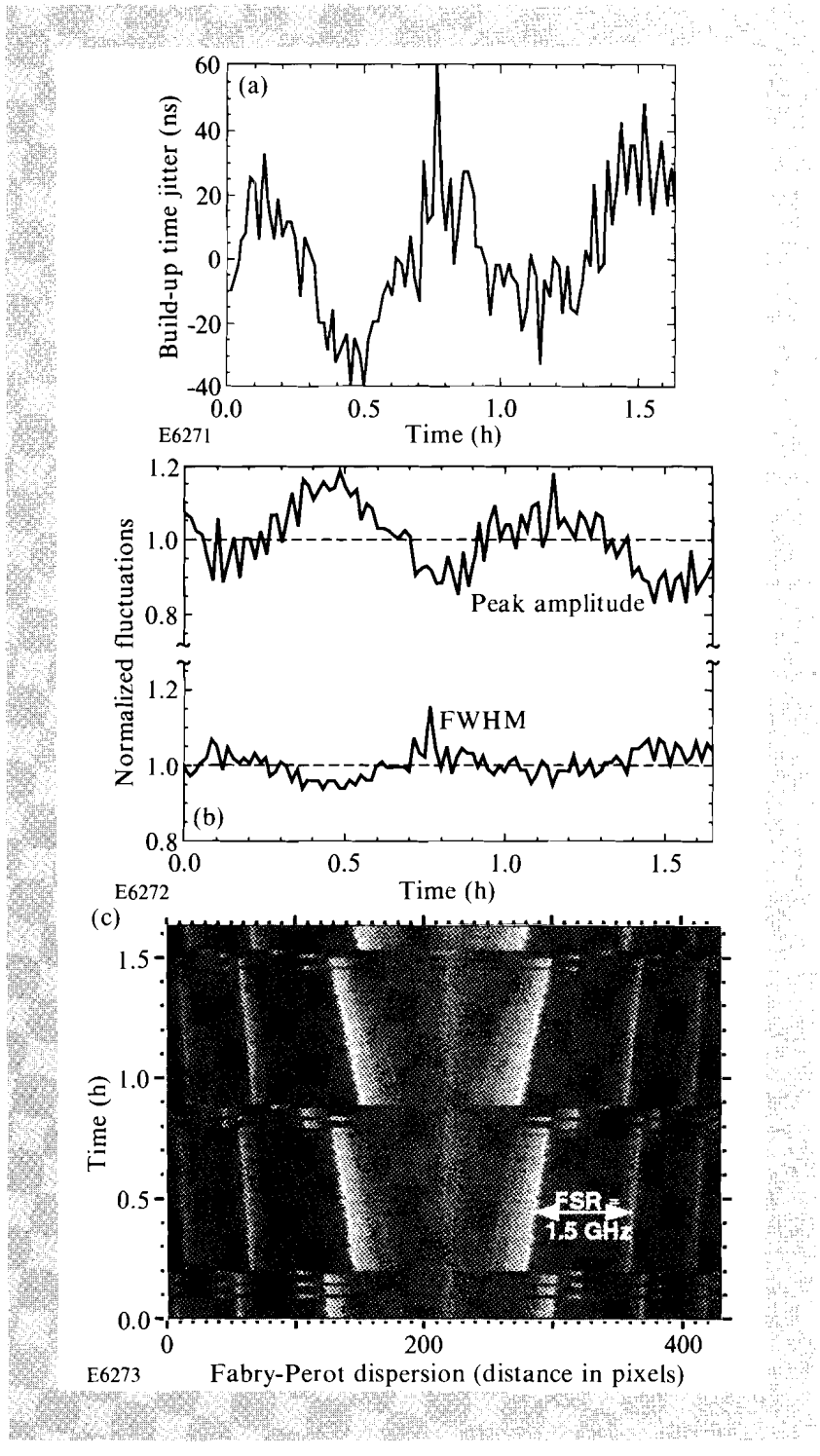

Fig. 51.31
Build-up time jitter (a), peak amplitude and FWHM fluctuations (b), and Fabry-Perot data (c) for mono-mode laser operation with intensity feedback control during the pre-lase phase, but without length stabilization. The gradual expansion of the optical path length (presumably caused by heating up of the active medium) is reflected in all three figures leading to mode-hopping and involving neighboring oscillator modes and neighboring intracavity etalon modes. Mode-hopping is accompanied by large build-up time jitter and significant amplitude fluctuations.

laser is again Q-switched ~40 μs into the pre-lase phase. Under these conditions, the laser tends to mode-hop roughly every 40 min because of an apparent constant change in temperature over the whole of the recording time. Close inspection indicates that around the time of mode-hopping the laser jumps several times between adjacent laser cavity and intracavity etalon modes before settling down on another laser-cavity mode. Ignoring for the moment the correlation between mode-hopping and the Q-switch pulse parameters, the fractional rms and peak-to-valley fluctuations [build-up time: 6% (30% p-t-v), FWHM: 4% (20% p-t-v), and peak amplitude: 9% (34%)] are noticeably larger for the mono-mode laser without length-feedback control. However, in none of the shots is there any evidence for the simultaneous presence of two modes as was observed in Figs. 51.27 and 51.28 where the feedback control was disabled and the pre-lase phase was ended at the top of the first relaxation oscillation. Thus, mono-mode operation by itself does not require active-length control of the oscillator but it is required for more reproducible Q-switch amplitude and build-up time performance.

Varying the length of the pre-lase phase before Q-switching beyond the time at which the relaxation oscillations are almost fully damped (~40 μs) degrades the build-up time jitter characteristics slightly (~5 ns additional jitter) while hardly affecting the amplitudes and FWHM of the output pulses or their standard deviations.

Summary

We have developed a highly reliable, reproducible, externally triggerable, single-mode, flash-lamp-pumped Nd:YLF laser system with negative, intracavity intensity feedback. Mono-mode operation can be maintained over periods of many hours. Adding another feedback control on the cavity length increases the output stability of the laser-pulse characteristics and forces lasing at a constant and selectable wavelength, also over periods of hours.

ACKNOWLEDGMENT

This work was supported by the U.S. Department of Energy Office of Inertial Confinement Fusion under agreement No. DE-FC03-85DP40200 and by the Laser Fusion Feasibility Project at the Laboratory for Laser Energetics, which is sponsored by the New York State Energy Research and Development Authority and the University of Rochester.

REFERENCES

1. Yu. D. Golyaev, A. A. Zadernovskiĭ, and A. L. Livintsev, Sov. J. Quantum Electron. **17**, 583 (1987); R. Roy, P. A. Schulz, and A. Walther, Opt. Lett. **12**, 672 (1987); W. A. Clarkson, A. B. Neilson, and D. C. Hanna, Opt. Lett. **17**, 601 (1992).
2. L. J. Bromley and D. C. Hanna, Opt. Lett. **16**, 378 (1991); W. A. Clarkson and D. C. Hanna, Opt. Commun. **81**, 375 (1991); W. A. Clarkson and D. C. Hanna, Opt. Commun. **84**, 51 (1991).
3. T. J. Kane and R. L. Byer, Opt. Lett. **10**, 65 (1985).
4. Y. K. Park, G. Giuliani, and R. L. Byer, Opt. Lett. **5**, 96 (1980); P. Esherick and A. Owyoung, J. Opt. Soc. Am. B **4**, 41 (1987).

5. D. J. Kuizenga, IEEE J. Quantum Electron. **17**, 1694 (1981); D. J. Kuizenga and A. E. Siegman, IEEE J. Quantum Electron. **6**, 694 (1970); D. J. Kuizenga and A. E. Siegman, IEEE J. Quantum Electron. **6**, 709 (1970); G. B. Michelangeli *et al.*, Opt. Commun. **65**, 283 (1988).

6. R. P. Johnson, N. K. Moncur, and L. D. Siebert, in *Proceedings of the International Conference on Lasers '87*, edited by F. J. Duarte (STS Press, McLean, VA, 1988), p. 432; I. N. Ross *et al.*, IEEE J. Quantum Electron. **17**, 1653 (1981).

7. D. C. Hanna, B. Luther-Davies, and R. C. Smith, Electron. Lett. **8,** 369 (1972); I. Will, Ph.D. Dissertation, Technische Universität Berlin, Berlin, Germany, 1991.

8. An alternative approach to cavity-length control has been reported by S. B. Darack, D. R. Dykaar, and G. T. Harvey, Opt. Lett. **16**, 1677 (1991).

9. J. E. Gibson, *Nonlinear Automatic Control* (McGraw-Hill, New York, 1963); "Translations of Papers on Stability of Nonlinear Feedback Control Systems," Natl. Bur. Stand. (U.S.), Spec. Publ. 1691 (U.S. Government Printing Office, Washington, DC, 1952); J. G. Truxal, *Automatic Feedback Control System Synthesis* (McGraw-Hill, New York, 1955), p. 566.